Macromolecules
ARTICLE

Macromolecules **2010**, *43*, 7625–7636 **7625**
DOI: 10.1021/ma1011733

High-Throughput Characterization of Novel PVDF/Acrylic Polyelectrolyte Semi-Interpenetrated Network Proton Exchange Membranes

Pedro Zapata,[†] David Mountz,[‡] and J. Carson Meredith*,[†]

[†]*School of Chemical & Biomolecular Engineering, Georgia Institute of Technology, Atlanta, Georgia 30332-0100, and* [‡]*Arkema Inc., 900 First Avenue, King of Prussia, Pennsylvania 19406*

Received May 27, 2010; Revised Manuscript Received July 28, 2010

ABSTRACT: The proton exchange membrane (PEM) is a fundamental component of the polymer electrolyte membrane fuel cell (PEMFC), a promising alternative energy conversion approach for low to medium power applications. Existing commercially available PEMs are based predominantly on perfluorosulfonic acid polymers (PFSA) (e.g., Nafion). In this study the viability of semi-interpenetrating ionomer−polymer networks from blends of poly(vinylidene fluoride) (PVDF) and covalently cross-linked sulfonated acrylic polyelectrolytes (PE) as potential PEMs is examined. A total of 80 PVDF/PE membranes, prepared from five different grades of Kynar PVDF (homo- and copolymers) and two types of PE, were characterized in terms of proton conductivity and mechanical properties using custom-developed high-throughput screening tools. In addition to PE type and content, the crystalline characteristics (i.e., crystallinity and crystallite size) and melt viscosity of the inert PVDF phase were found to have a major effect on proton conductivity. Particularly, membranes based on the most highly crystalline and viscous PVDF homopolymers exhibited the lowest proton conductivity, associated with reduced segmental motion of PE chains during membrane formation. Mechanical properties of the membranes were dominated by the properties of PVDF. Membranes based on higher modulus PVDF homopolymers exhibited higher elastic modulus and tensile strength, while those based on the more flexible poly(vinylidene fluoride-co-hexafluoropropylene) (PVDF:HFP) copolymers exhibited enhanced toughness. In general, the resulting PVDF/PE membranes compared favorably to Nafion, having conductivities in excess of 130 mS/cm (vs 84.5 mS/cm for Nafion) and mechanical properties 2−5 times higher in some cases. While the selection of a unique conductivity and mechanical properties combination is impractical in view of the fact that requirements are dictated by the final application of the membrane, PVDF/PE semi-interpenetrated network membranes hold very good promise for PEMFC applications.

Introduction

Fuel cells are anticipated to be a basic building block in the transition toward a more sustainable energy economy in the 21st century.[1−5] The use of fuel cells is envisioned in applications that range from portable electronics to transportation to stationary power generation. In the small to medium power markets (e.g., personal electronics and light duty vehicles), proton exchange membrane fuel cells (PEMFCs), also referred to as polymer electrolyte membrane fuels cells, have garnered a great deal of attention.[1,2,6]

The PEM serves as a solid electrolyte barrier to separate the fuel and oxidant streams, while providing a path for transport of protons resulting from anodic oxidation of the fuel. The PEM has to meet numerous requirements for robust fuel cell operation and has become one of the performance-limiting components in PEMFCs. Among these requirements are high proton conductivity, low electronic conductivity, low permeability to both fuel and oxidant, low water transport, high hydrolytic stability under the oxidative fuel cell environment, and excellent mechanical integrity, not to mention competitive cost.[3,7−11]

Perfluorosulfonic acid (PFSA) polymer electrolyte membranes have been the platform of choice for the development of PEMFCs in the past;[7,8,11] however, PFSA-based membranes are expensive and have operational limitations such as high fuel crossover and relatively poor mechanical integrity in the hydrated state.[7,8] Extensive research is underway to address these limitations and meet the aforementioned PEM requirements in order to devise affordable materials with enhanced performance and extended lifetime. Although much fuel cell engineering still focuses on PFSA-based membranes, present-day PEM research also involves the development of alternative PEM materials based on the functionalization, particularly sulfonation, of high-performance hydrocarbon polymers such as polyimides (PI), poly(ether ether ketone)s (PEEK), poly(ether sulfone)s (PES), polybenzimidazole (PBI), and other polyaromatics.[8] A different approach that can provide a potential cost-effective alternative to PFSA membranes involves the blending of a proton-conducting component with a stable and mechanically sound inert component (generally an engineering thermoplastic) that provides improved mechanical and thermal stability to the membrane.[7,12−14]

Although less common than sulfonation strategies, polymer blending is gaining ground as a promising methodology for the development of PEMs. Recent studies have shown the feasibility of this approach, including PEMs based on methyl methacrylate (MMA) compatibilized poly(vinylidene fluoride) (PVDF) and styrene−ethylene/butylene−styrene (SEBS) blends;[15] poly(2,6-dimethyl-1,4-phenylene oxide) (PPO) acid−base blends;[16]

*To whom correspondence should be addressed: Tel +1 404 385 2151; Fax +1 404 894 2866; e-mail carson.meredith@chbe.gatech.edu.

Published on Web 08/13/2010

sulfonated poly(arylene ether), PES, and polysulfone (PSF), or PBI blends;[14] sulfonated poly(ether ketone ketone) (SPEKK) and PES (or SPEKK with a different sulfonation level) blends;[13] and poly(styrene-*b*-vinylbenzylphosphonic acid) (PS-*b*-PVBPA) and PPO blends.[12] The key advantage of polymer blending resides in the ability to combine the properties of two or more different polymers, which in turn can result in a decoupling of mechanical and proton-conducting properties. Moreover, the use of accessible commercial polymers is an added advantage since synthesis of new polymers is not required, thus reducing the costs associated with the development of new PEM materials.

PVDF is a commercially available and widespread engineering thermoplastic that is resistant to highly oxidative and extreme acidic environments and has exceptional electrochemical stability and mechanical toughness, making it an excellent candidate as the inert, mechanically robust matrix for blended PEMs. In fact, PVDF has been recently used in PEM designs including blending with SEBS[15] and in PVDF-supported poly(methacrylic acid) and poly(*p*-styrenesulfonic acid) membranes.[17] Its suitability as a porous support for direct methanol fuel cell PEMs has also been assayed.[18] In addition to its use in relevant applications, the choice of PVDF, as opposed to a hydrocarbon-based thermoplastic, is motivated by a desire to retain the chemical resistance of a perfluorinated polymer, while utilizing a material that is commercially available at a lower cost. While a significant literature already has evaluated a large number of hydrocarbon engineering thermoplastics as components in blends with polyelectrolytes,[8−16] considerably less work has studied PVDF as a PEM component.

In this work we evaluate the feasibility of ionomer−polymer semi-interpenetrated networks (SIPN) obtained by blending PVDF (inert matrix, mechanical support phase) and covalently cross-linked sulfonated acrylic polyelectrolytes (PE) (proton-conducting phase) as potential PEM material candidates. In particular, proton-conducting and mechanical properties are examined for a wide variety of membranes based on two types of acrylic polyelectrolytes of different equivalent weight and multiple PVDF grades. We have selected commercially available types of PVDF, sold under the trade name Kynar, for evaluation in blends with PEs. Two PVDF homopolymers, one with approximately twice the molecular mass of the other (Kynar 500 and Kynar 731), and three random PVDF:HFP copolymers (Kynar 2801, Kynar 2821, and Kynar 2851), which vary the relative amount of HFP, have been chosen. The variation in molecular mass and HFP content leads to differences in crystallinity, glass transition temperature, and crystallite size that are expected to influence the formation of proton conducting channels in blends with PEs.

Exploratory research comprising *de novo* material syntheses generally involves extensive variable spaces that encompass both material properties and processing conditions. To alleviate this burden, high-throughput screening techniques are utilized for the characterization of PVDF/PE membranes. Namely, high-throughput mechanical characterization (HTMECH)[19] and high-throughput conductivity (HTC)[20] methods, described in detail previously, were used. High-throughput methods have been recently utilized in the fuel cell area in the study of catalysts for use in PEMFCs,[21] and a comprehensive application of these techniques to the study of other PEMFC components such as the proton exchange membrane can offer significant cost and efficiency advantages to the discovery and optimization stages of the global PEMFC design and development process.

Experimental Section

Membrane Preparation, Protonation, and Conditioning. Proton-conducting SIPN membranes were prepared from numerous grades of Kynar poly(vinylidene fluoride) (PVDF) and two dissimilar novel sulfonated acrylic polyelectrolytes (PE) consisting of a random copolymer of 2-sulfethyl methacrylate (SEM) (69 wt %), 2-hydroxyethyl methacrylate (HEMA) (15 wt %), methyl methacrylate (MMA) (8 wt %), and styrene (7 wt %) in the case of polyelectrolyte no. 1 (PE1) and a random copolymer of SEM (90 wt %) and HEMA (10 wt %) in the case of polyelectrolyte no. 2 (PE2) (Figure 1). PMMA and PS were included in the polyelectrolyte in order to incorporate nonfunctional (e.g., non-sulfonated, non-hydroxylated) components in the polyelectrolyte backbone. These act primarily as nonionic and nonreactive (relative to isocyanate cross-linker) "spacers" that adjust the fraction of sulfonated groups. PMMA was chosen due to its well-known miscibility with PVDF, and PS was chosen as a simple hydrophobic, immiscible component. The selection of the various percentages of PMMA and PS was based on the ability to achieve maximum conductivity in an experimental design screening. The different Kynar PVDF grades utilized, specifically Kynar 500 (M_w = 523 000 g/mol; H−H defect = 11.6%),[22] Kynar 731 (M_w = 260 000 g/mol; H−H defect = 10%),[22] Kynar 2801 (M_w = 380 000 g/mol; PVDF:HFP = 88:12 molar ratio),[23,24] Kynar 2821 (PVDF:HFP = 88:12 molar ratio), and Kynar 2851 (M_w = 455 000 g/mol; PVDF:HFP = 95:5 molar ratio)[22] (all in a fine powder form) (supplied by Arkema Inc., Kynar is a registered trademark of Arkema Inc.) were dissolved in 1-methyl-2-pyrrolidinone (NMP) (Sigma-Aldrich Co., assay ≥99.5%) to a total concentration of 10 wt % per solution. These solutions were mixed at multiple PVDF to PE ratios with individual stock solutions (25 wt % total solids in NMP) of each polyelectrolyte. PVDF/PE mixtures were combined with Desmodur N-3300A (Bayer AG), a 1,6-hexamethylene diisocyanate-derived triisocyanate cross-linker, at a 1:0.8 OH:NCO ratio for PE1 and 1:0.9 OH:NCO ratio for PE2 (80 and 90 mol % of the stoichiometric amount of cross-linker needed to react with all the polyelectrolyte hydroxyl groups, respectively). The final blends were thoroughly mixed at room temperature under an inert nitrogen atmosphere for ∼30 min, followed by a brief degassing by sonication (∼5 min) before film coating. Coating was performed using a knife-edge apparatus[25,26] to spread liquid PVDF/PE films onto silicon ⟨100⟩ substrates (Silicon, Inc.) previously cleaned for 2 h in piranha solution (70 vol % H_2SO_4, 9% H_2O_2, 21% H_2O) at 80 °C. The resulting films were cured at 175 °C for 20 min in a forced convection oven to cross-link the PE and remove excess NMP. Conversion of isocyanate groups into urea linkages was estimated via Fourier transform infrared (FT-IR) spectroscopy (Experimental Section) by tracking the disappearance of the −NCO peak (2260 cm^{-1}) in order to confirm the completeness of the PE cross-linking reaction. Cured PVDF/PE membranes were detached from the silicon substrates by immersion in DI water at room temperature. Composition of final membranes ranged from 25 to 65 wt % neutralized form PE (equivalent to 17 to 48 wt % acid form PE in the case of PE1 and 15 to 44 wt %

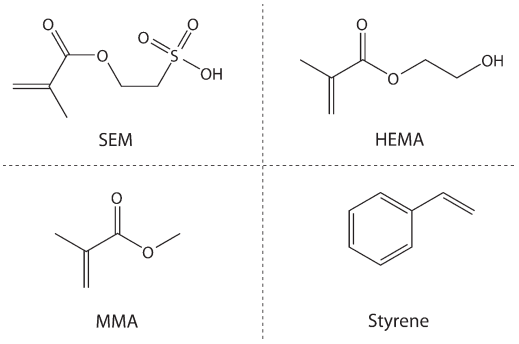

Figure 1. Acrylic polyelectrolyte monomers. PE1: SEM (69 wt %) + HEMA (15 wt %) + MMA (8 wt %) + styrene (7 wt %). PE2: SEM (90 wt %) + HEMA (10 wt %).

acid form PE in the case of PE2) for each grade of Kynar PVDF and each PE.

Prior to protonation, free-standing membranes were washed in a 1 M HCl solution at 80 °C for 2 h, followed by a 15 min rinse in DI water. The acid-washed membranes were protonated by immersion in 1 M H_2SO_4 at 80 °C for 2 h, followed by removal of excess sulfuric acid by several successive 15 min rinses in DI water until the pH of the rinse water was above 4. Conditioning of protonated PVDF/PE membranes as well as Nafion 112 standards used as reference was carried out by immersion in boiling 18.2 MΩ water for 1 h to allow complete membrane swelling. Swollen membranes were stored in 18.2 MΩ water until conductivity measurements were performed.

High-Throughput Conductivity Measurement. Proton conductivity measurements were performed by AC electrochemical impedance spectroscopy (EIS) using a custom fully automated high-throughput conductivity measuring device (HTC).[20] Briefly, the conditioned membrane to be tested is placed in an electrically insulating sample holder and held in place with a grid retention mechanism. The sample holder assembly is filled with 18.2 MΩ water to fully cover the membrane and avoid dehydration. The water-immersed membrane is excited via a small AC signal using a miniature 4-point probe (point-contact collinear electrodes) that creates a dipole source with cylindrically symmetric isocurrent surfaces within the membrane. The response voltage is measured via the inner point electrodes, which allows determining the membrane complex impedance. Proton conductivity is estimated from the calculated complex impedance by means of the following model:

$$\sigma|_{Z'' \to 0} \approx -\frac{1}{Z_{(jw)} 2\pi h}\left[\ln\left(\frac{x_1}{x_2 + x_3}\right) - \ln\left(\frac{x_1 + x_2}{x_3}\right)\right] \quad (1)$$

where σ is the membrane proton conductivity, $Z_{(jw)}$ is the membrane complex impedance, h is the membrane thickness, and x_i are the interelectrode distances of the 4-point probe.

Conductivity measurements for all membranes, including Nafion 112 standards, were performed using the HTC in potentiostatic mode with an excitation signal of 1000 Hz and 30 mV (~20 mV rms) and a response signal integration time of 5000 cycles following a 5 s stabilization period.

High-Throughput Mechanical Property Measurement. Characterization of PVDF/PE membranes mechanical properties was performed using an automated modified high-throughput mechanical testing apparatus (HTMECH) based on a previous design.[19] A general overview of the process is as follows: the membrane is mounted on a sample holder consisting of a pair of gridlike steel isolation plates affixed to a linear motor. The holder/membrane assembly is moved at a predefined speed toward a hemispherical-tip shaft connected to a high-sensitivity load cell. As the membrane is indented by the shaft or "needle", the force exerted on load cell is recorded, generating a force vs time profile that depicts the evolution of the membrane axisymmetric biaxial deformation and fracture process. To assess the true mechanical response of the membranes (e.g., elastic modulus, tensile strength, elongation at break, and toughness) the measured force vs time profiles undergo denoising, conditioning and analysis via a custom-developed algorithm. Specifically, artifacts arising from background noise, natural vibration frequencies of the system, and harmonic oscillations from the motion of the linear motors, are minimized via undecimated wavelet transforms and noncausal zero-phase IIR filters. Characterization of conditioned signals is accomplished via profile scaling and second-derivative techniques. As otherwise stated, denoising of all raw profiles was carried out via either undecimated wavelet transform with multiple-level rescaling to estimate noise variance (noise was not assumed white), universal threshold, and an orthogonal Haar wavelet type or a noncausal zero-phase IIR filter using first order Chebyshev coefficients, a passband ripple of 0.2−0.3 dB, and a cutoff frequency of 10 Hz. Bisquare fitting sensitivity was set to 95% for linear fitting of elastic modulus.

Mechanical characterization tests for all membranes and Nafion 112 standards were performed at a constant speed of 10 mm/s using a 1.24 mm diameter needle (needle to isolation plate hole diameter ratio: 0.413). Sampling rate of the load cell signal was set to 5000 samples/s. All membranes were tested in a fully hydrated state.

PVDF and Membranes Characterization. *Differential Scanning Calorimetry* (*DSC*). Thermal characterization of PVDF powders via DSC was carried out using a DSC Q20 (TA Instruments). PVDF samples (≈5 mg each), enclosed in hermetic aluminum pans, were subjected to three temperature cycles (heating−cooling−heating), within a temperature interval of −40 to 200 °C, at a heating/cooling rate of 10 °C/min. All tests were performed under an inert nitrogen atmosphere.

X-ray Diffraction (*XRD*). X-ray diffraction spectra of PVDF powders and proton conducting membranes were recorded using a PANalytical X'Pert PRO diffractometer (PANalytical). The incident beam configuration consisted of a Cu-anode tube (λ Cu Kα_1 = 1.540 598 Å, λ Cu Kα_2 = 1.544 426 Å) operated at 45 kV and 40 mA with a fixed 1/16° (0.19 mm) divergence slit, a 0.04 rad Soller slit, and a nickel β-filter to remove Cu Kβ radiation. The detector, a PANalytical X'Celerometer, was equipped with a 10 mm antiscatter slit and a 0.04 rad Soller slit. Data were collected over a 2θ range of 2°−70° at an equivalent scan rate of ~0.047 deg/min (0.008° scan step size, 10.16 s/step).

Fourier Transform Infrared Spectroscopy (*FT-IR*). Infrared absorption spectra of PVDF films and proton conducting membranes were collected at room temperature with a Bruker IRscope II (Bruker Optics Inc.) for reflection mode and a Bruker Equinox 55 spectrometer (Bruker Optics Inc.) for transmission mode, both coupled with a KBr beam splitter. The spectra were recorded in the range of 400−5000 cm^{-1} at a resolution of 4 cm^{-1} and averaged 128 times.

Scanning Electron Microscopy (*SEM*). High-resolution images of proton conducting membranes were obtained using a LEO 1530 thermally assisted field emission scanning electron microscope (LEO Electron Microscopy Group), operated at 10 keV. Samples for SEM imaging were prepared by cryogenic facture in liquid nitrogen followed by vacuum metallization with gold.

Statistical Analysis. An unbalanced univariate general linear model (GLM) (2- and 3-way, type III sums of squares) was used for evaluation of significant factors; $p < 0.05$ was defined as significant (5% significance level). Levene's test was used to determine data sets homogeneity of variance (homoscedasticity), while data sets normality was assessed using the Shapiro-Wilk test. Pairwise comparisons of significant factors from 3-way GLM tests were performed by comparisons of unweighted means of main effects with Sidak-adjusted confidence intervals, while Tamhane's T2 post hoc test was utilized for pairwise comparisons of significant factors from 2-way GLM tests. All results are expressed as mean ± standard error of the mean (±SEM) or as mean ±95% confidence intervals.

Results and Discussion

Proton Conductivity. Proton conductivity from HTC screening of 80 PEM candidates, prepared from various Kynar PVDF grades and acrylic PE fractions, is shown in Figure 2. There is an apparent correlation between conductivity and PE content for both polyelectrolytes and each Kynar grade. Also revealed is the dissimilarity between membranes containing one or the other polyelectrolyte and how these PVDF/PE membranes compare to Nafion 112 (semitransparent planes in Figure 2A,B) at identical testing conditions. PE2-based membranes compare more favorably to Nafion 112 as they reach similar or higher conductivities

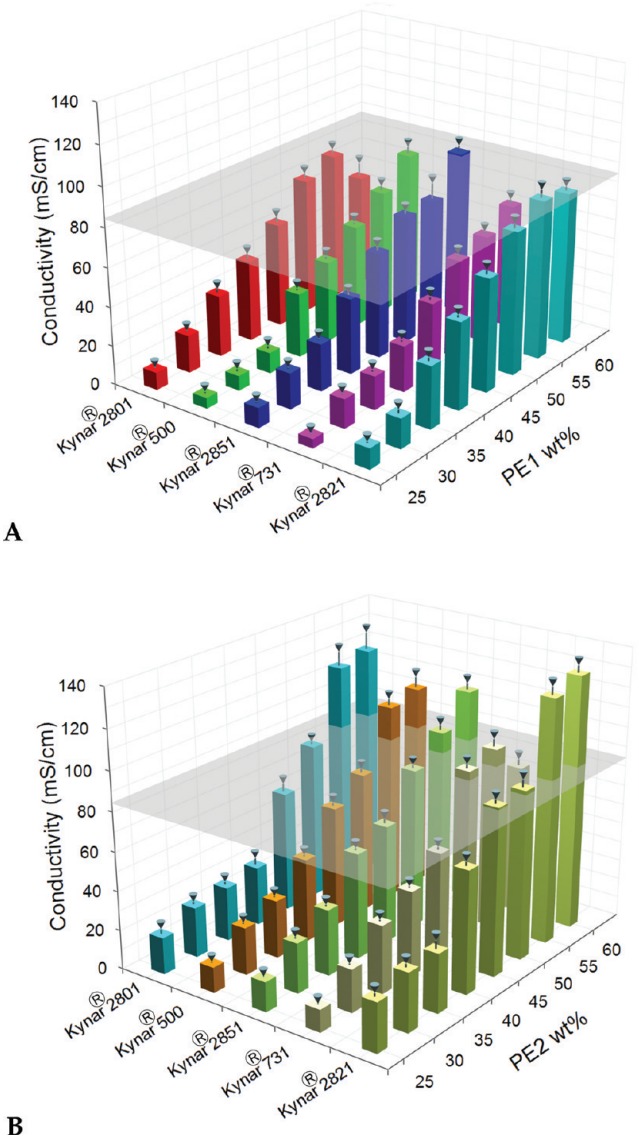

Figure 2. Conductivity of Kynar PVDF/acrylic polyelectrolyte membranes for various Kynar grades and PE mass fractions. Polyelectrolyte content is expressed as the weight percentage of neutralized form polyelectrolyte in the final membrane. (A) PE1-based membranes; range: 25−60 wt % neutralized form PE1 (equivalent to approximately 17−48 wt % acid form PE1). (B) PE2-based membranes; range: 25−60 wt % neutralized form PE2 (equivalent to approximately 15−44 wt % acid form PE2). Test conditions: 18.2 MΩ water at 25 °C. Excitation signal: 1000 Hz, 30 mV. Semitransparent planes correspond to the average conductivity of Nafion 112 (84.5 ± 0.54 mS/cm[20]) at identical testing conditions. Values are averages ± SEM (indicated by error bars delimited with inverted cone markers) (n = 2−24 for PE1, n = 4−16 for PE2).

(up to 25−30 mS/cm more in some cases) than Nafion at PE2 contents of 45 wt % and above. Conversely, only PE1 membranes containing Kynar 2821 or 2851 attain conductivities as high as Nafion 112. In general, membranes containing PE2 exhibit higher conductivity than their PE1 counterparts at identical PE mass fraction, as expected from the lower equivalent weight of the former (280 g PE1/mol SO_3H for PE1 vs 216 g PE2/mol SO_3H for PE2). However, differences in conductivity between membranes are not due only to the PE content but also appear to be influenced by the PVDF grade. To evaluate the effect of these factors on the PVDF/PE membranes properties in a quantitative manner, the conductivity data were analyzed using an unbalanced GLM. As anticipated, the PE content and PE type have a major effect on proton conductivity. The analysis revealed statistically significant effects of PE content ($F_{(7,815)} = 1154$, $p < 0.001$) and PE type ($F_{(1,815)} = 807.9$, $p < 0.001$) related to the aforementioned equivalent weight difference between the polyelectrolytes. A significant effect of PVDF grade on proton conductivity was also evident ($F_{(4,815)} = 84.5$, $p < 0.001$). Interestingly, an η_{p^2} statistic, which reports the "practical" significance of a factor on the dependent variable, of 0.293 indicates a considerable effect of PVDF grade; that is, PVDF grade by itself accounts for about 30% of the overall variance. Statistically significant interactions between the main effects PE type and PVDF grade ($F_{(4,815)} = 6.37$, $p < 0.001$), PE content and PVDF grade ($F_{(28,815)} = 6.7$, $p < 0.001$), and PE type and PE content ($F_{(7,815)} = 38.29$, $p < 0.001$) were also present. Simple main effects tests performed separately at fixed levels of the significant factors verified these statistical interactions, including the influence of PVDF grade on proton conductivity for PE1 contents above 30 wt % ($4.92 \le F_{(4,815)} \le 18.1$, $p < 0.001$) and PE2 contents above 35 wt % ($6.97 \le F_{(4,815)} \le 56.0$, $p < 0.001$); the effect of PE type for all PVDF types (particularly for PE contents of 35 wt % and above) ($4.26 \le F_{(1,815)} \le 250.9$, $p < 0.001$); and the impact of PE content at all levels of PVDF grade and PE type. That a statistical interaction between main effects for PE and PVDF types exists is perhaps not surprising, given the known molecular interactions of PVDF with carbonyl-containing polymers.[27]

Pairwise comparisons by unweighted means of PE content at a 5% significance level ($\alpha = 0.05$) showed that conductivity of membranes with a PE content of 55 and 60 wt % are statistically indistinguishable ($p = 0.661$), regardless of the polyelectrolyte type. This is in line with our previous findings from membranes based solely on PE1[20] and suggests the existence of an optimal amount of PE content in the vicinity of 55−60 wt %, above which any gain in proton conductivity is marginal. Presumably, this effect is associated with the coalescence of PE chains observed by SEM at high PE fractions (Figure 3). PE coalescence may be related to the neutralization degree of the polyelectrolyte (for this particular study both polyelectrolytes have a degree of neutralization of 0.95). At elevated PE concentrations the unneutralized sulfonic acid groups have higher probability of coming in close range one to another before covalent crosslinking of the PE, resulting in the coalescence of PE chains to form PE clusters. This is consistent with slight haziness observed for membranes with elevated PE content.

Pairwise comparisons of unweighted means of PVDF type exposed an interesting result: the presence of four homogeneous subsets where only Kynar 2851 and 2801 constituted a subset with more than one Kynar grade. Previously, in our study of PVDF/PE1 membranes,[20] the homogeneous subsets coincided with the family to which each PVDF type belonged; that is, membranes containing PVDF:HFP copolymers (Kynar 2801, 2821, and 2851) constituted one homogeneous subset, while those containing PVDF homopolymers (Kynar 500 and 731) each constituted a separate subset. The departure of Kynar 2821 from a homogeneous subset for PE1-based membranes to an individual subset for PE2-based membranes is readily seen in Figure 4, which displays the comparison of global and individual (PE1 and PE2) unweighted means of conductivity by PVDF type. This divergence is not completely unexpected as it is supported by the aforementioned significant interaction effect between PE type and PVDF grade. It is important to notice that the overall trend of unweighted means depicted in Figure 4 is almost identical for both polyelectrolytes. This similarity is a

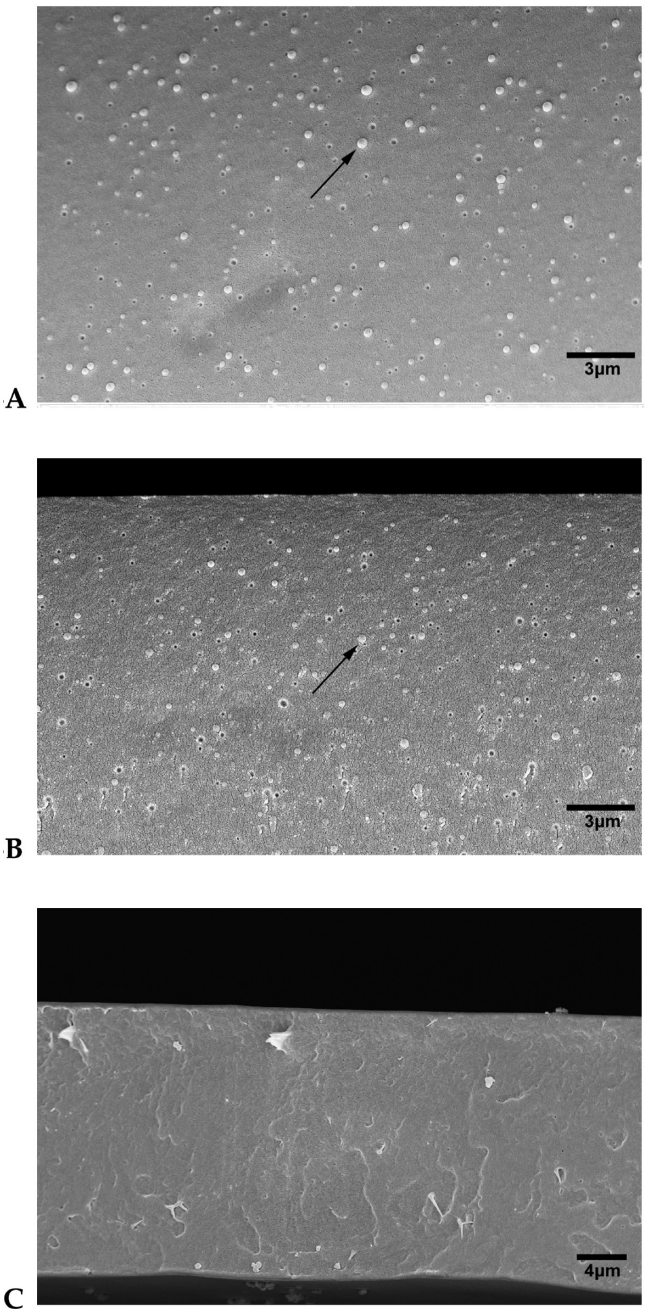

Figure 3. SEM images of the cross-sectional area of PVDF/PE membranes, EHT 10 kV. High PE: 60 wt % (neutralized form PE) (A) Kynar 2851/PE1 and (B) Kynar 500/PE2. Low PE: 25 wt % (neutralized form PE) (C) Kynar 2801/PE1. Arrows in (A) and (B) indicate representative PE clusters resulting from the coalescence of PE chains. Only one representative image per polyelectrolyte type is shown at high PE to visualize the difference between clusters of each PE type. Low PE image is provided as contrast due to the absence of PE clusters (artifacts in the image are the result of the cryogenic fracture).

clear indicator that membrane proton conductivity is closely related to the PVDF properties and that the effect of a specific PVDF grade on conductivity is comparable across all acrylic polyelectrolytes used. For instance, regardless of the PE type, high proton conductivity was favored in membranes containing PVDF:HFP copolymers when compared to those containing PVDF homopolymers. Furthermore, the highest conductivity always corresponded to membranes based on Kynar 2821, while the lowest to those based on Kynar 731.

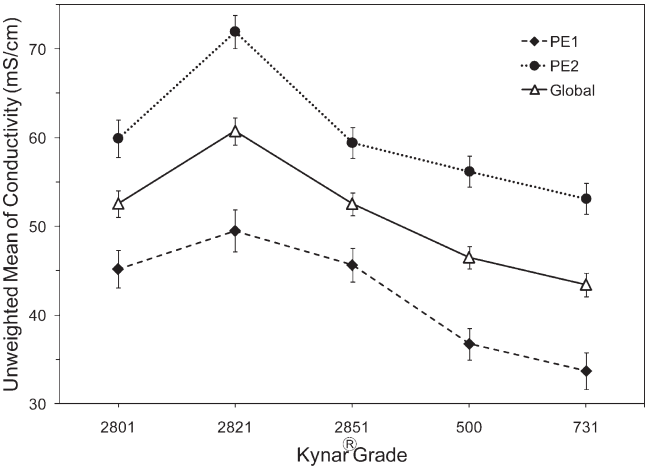

Figure 4. Unweighted means of conductivity as a function of Kynar grade estimated from 2-way (PE1 and PE2 profiles) and 3-way (global profile) univariate unbalanced GLM analysis (full factorial model).

PVDF is an extensively studied semicrystalline polymer known for the complex polymorphism of its crystalline phase.[28−33] There are at least four known PVDF crystal phases: namely, α (phase II), β (phase I), γ (phase III), and δ (phase IV or polar phase II), which are dependent on numerous factors, including mechanical and thermal history as well as processing conditions. Furthermore, it is known that the use of a comonomer such as HFP can disrupt the ordering of the PVDF chains, thus reducing its degree of crystallinity.[28,34,35] The degree of crystallinity and type of crystalline phase of PVDF can affect its bulk properties (e.g., mechanical strength, glass transition, and melting temperatures) as well as its interaction with other polymers (e.g., miscibility, phase separation). Information about crystallinity of the different PVDF grades can be obtained directly from their corresponding XRD spectra shown in Figure 5A. All the spectra exhibit similar semicrystalline morphologies with a broad amorphous halo and crystalline reflections located at the following scattering angles (2θ): 18.34 ± 0.07°, 19.89 ± 0.07°, and 26.61 ± 0.14° (Table 1). These locations are associated with the reflections (020), (110), and (021) typical of the PVDF α-phase.[31−33,36,37] This indicates that the crystalline phase type for both homopolymer and copolymer samples is identical and that differences in crystallinity among them are likely due to the size and amount of crystallites. XRD spectra were baseline-corrected and smoothed using a fast Fourier transform (FFT) filter, followed by Voigt and Gaussian peak fitting (Peakfit, Systat Software Inc.) to deconvolute the crystalline peaks from the amorphous halo. The size of coherently diffracting crystalline domains (crystallites) was approximated from the broadening of their diffraction peaks via Scherrer's equation (eq 2)[35] (ignoring instrument-related peak broadening effects):

$$D = \frac{K\lambda}{\beta_{2\theta} \cos \theta_0} \tag{2}$$

where D is the average crystallite size perpendicular to a particular hkl plane, $\beta_{2\theta}$ is the angular width at half-maximum of the peak associated with the hkl plane, θ_0 is the peak centroid Bragg angle, λ is the Cu Kα wavelength, and K is the Scherrer shape factor (taken as ~0.94, assuming that a cube-shaped monodisperse crystallite model is valid for the general case). Overall, calculation of crystallite size was robust to ambiguities of the peak fitting and deconvolution process,

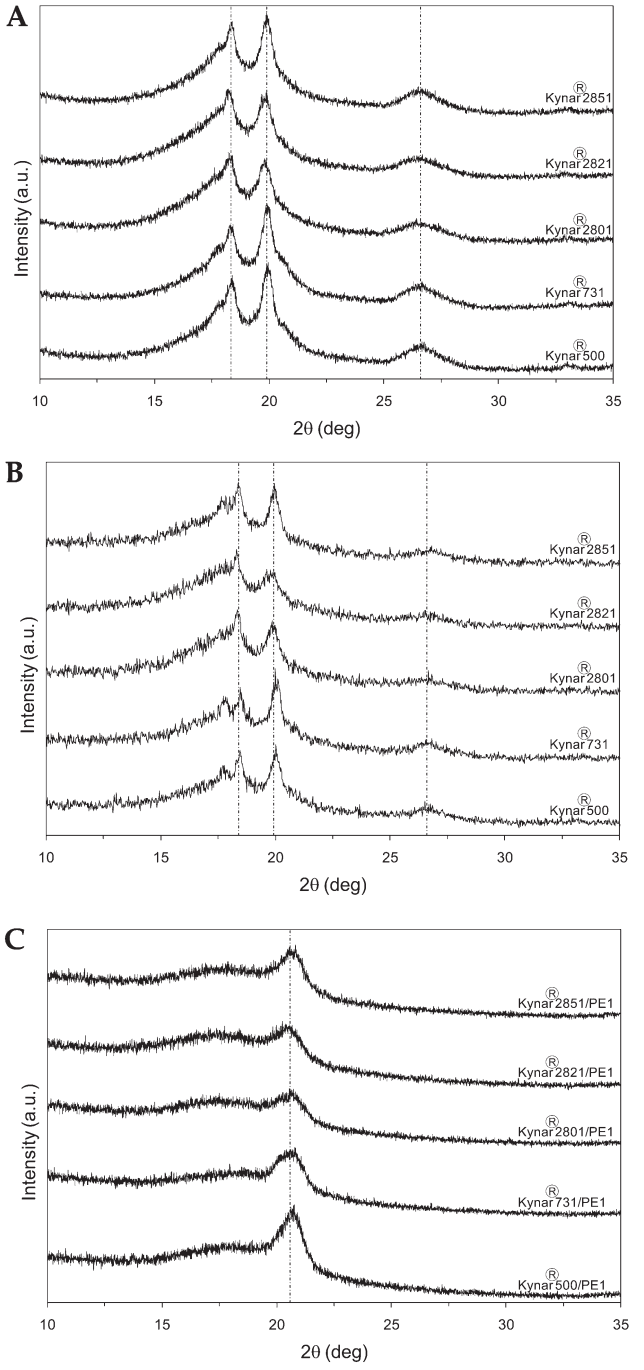

Figure 5. Wide-angle X-ray diffraction spectra. (A) Kynar PVDF powders (as received from the manufacturer). (B) NMP solvent-cast Kynar PVDF films. (C) Kynar PVDF/PE1 membranes (only representative spectra of membranes containing 50 wt % neutralized form PE1 are shown; membranes containing PE2 and different PE mass fractions exhibited identical behavior). Vertical lines in (A) and (B) indicate α-phase crystalline reflections at scattering angles (2θ) 18.34° (020), 19.89° (110), and 26.61° (021). Vertical line in (C) indicates a β-phase crystalline reflection at a scattering angle (2θ) of 20.58° (110) + (200). Spectra in (B) and (C) are not corrected for sample thickness.

revealing smaller crystallites in the matrix of the PVDF copolymers than in the homopolymers (Table 1). The smallest crystallites correspond to Kynar 2821 (152.4 Å), while the largest to Kynar 731 (200.2 Å). Conversely, crystallinity fluctuated considerably depending on the data processing and spectral decomposition; as a result, it was quantified via DSC.

Table 1. Wide-Angle X-ray Diffraction (WAXD) of Pure PVDF Powders[a]

	hkl (020)		*hkl* (110)		*hkl* (021)		
PVDF grade	2θ (deg)	d (Å)	2θ (deg)	d (Å)	2θ (deg)	d (Å)	D (Å)[b]
Kynar 500	18.38	4.83	19.95	4.45	26.75	3.33	183.58
Kynar 731	18.43	4.82	19.96	4.45	26.70	3.34	200.15
Kynar 2801	18.27	4.86	19.80	4.49	26.44	3.37	164.56
Kynar 2821	18.27	4.86	19.89	4.47	26.69	3.34	152.36
Kynar 2851	18.38	4.83	19.89	4.47	26.50	3.36	159.55

[a] θ = Bragg angle, d = interplanar spacing, and D = crystallite size approximation from Scherrer's equation. [b] Crystallite sizes derived from baseline-corrected (110) crystalline reflections.

Table 2. Thermal Characteristics of Pure PVDF Powders (DSC)[a]

PVDF grade	T_m (°C)	ΔH_f (J/g)	X_C (%)
Kynar 500	162.39	53.07	50.69
Kynar 731	169.05	72.30	69.05
Kynar 2801	146.68	38.83	37.09
Kynar 2821	144.85	25.96	24.79
Kynar 2851	158.31	51.07	48.78

[a] T_m = melting peak temperature and ΔH_f = enthalpy of fusion. Heating and cooling rates were 10 °C/min.

Estimation of the Kynar PVDF crystallinity was carried out using the following simple model (a more rigorous approach can be found elsewhere[36]):

$$X_C\ (\%) = \frac{\Delta H_f}{\Delta H_m^0} \times 100 \qquad (3)$$

where ΔH_f is the enthalpy of fusion of the PVDF sample calculated by integration of the fusion endotherms of the DSC heating profiles (presented in Supporting Information, Figure S1) and ΔH_m^0 is the standard enthalpy of fusion of 100% crystalline PVDF. In lieu of individual standard enthalpies of fusion for each of the PVDF grades, a typical accepted value of 104.7 J/g[36,40] was used instead. Hence, the crystallinities calculated should only be interpreted as *relative* values for use in comparing the relative crystallinity of samples prepared at identical conditions in this study. The lack of exothermic recrystallization peaks in all DSC profiles indicates no additional heat-induced crystallization of the amorphous phase; therefore, no further adjustment of the calculated enthalpies of fusion was necessary. Crystallinity values, along with thermal characteristics including fusion enthalpies and melting temperatures, are presented in Table 2. Following the same trend of crystallite size, copolymers exhibit a lower degree of crystallinity than the homopolymer counterparts. Particularly, Kynar 2821 is ranked at the bottom with the smallest crystallites and lowest crystallinity (152.4 Å and 24.8%); in addition, it also has the lowest melting and crystallization temperatures (144.9 and 97.2 °C). In contrast, Kynar 731 has the largest crystallites and highest crystallinity (200.2 Å and 69.1%), in addition to the highest melting and crystallization temperatures (169.1 and 135.2 °C).

Remarkably, the aforementioned proton conductivity trends follow the exact opposite behavior; that is, Kynar 2821-based membranes have the highest average conductivity, while those containing Kynar 731 have the lowest conductivity. This relationship applies as well for the PVDF grades in between, with conductivity decreasing as crystallinity, crystallite size, and melting and crystallization temperatures increase (Figures 6 and 7). Furthermore, the end of the Kynar 731 fusion endotherm is slightly above the curing temperature of the membranes (~177−178 °C vs 175 °C), indicating that the Kynar 731 is not completely melted

during the curing process. This may indicate a competition between PVDF crystallization and PVDF−PE phase separation that restricts the formation of ion conducting channels, explaining in part the lower conductivity of Kynar 731-based membranes.

Additional XRD spectra of pure PVDF solvent-cast films from NMP (175 °C, 20 min) and PVDF/PE membranes are shown in parts B and C of Figure 5, respectively. The locations of the crystalline peaks in the neat PVDF film spectra show that upon cooling from the molten state all the PVDF grades crystallize back to the α-phase (scattering angles (2θ): 18.4 ± 0.06°, 19.93 ± 0.1°, and 26.61 ± 0.12°, Table 3). This is supported by FT-IR spectra of the PVDF films (Figure 8A) which exhibit well-defined α-phase absorption bands at 408, 489, 614, 764, 796, 855, 976, and 1070 cm^{-1},[31,32,41] as well as the nonpolar trans−gauche CF_2 bending at 532 cm^{-1}, with no evidence of β or γ crystals—behavior consistent with previous studies where the α-phase is predominant when PVDF is cooled from the melt.[31,32,42] Despite crystallizing to the same phase type as the original PVDF powders, it is important to notice that the broader and shallower crystalline reflections (from baseline corrected XRD spectra) indicate a strong effect of the fast quenching of the films (175 °C to room temperature in less than 30 s) on their crystallinity and crystallite size (i.e., reduced crystallinity and smaller crystallites). Contrary to PVDF-only films, PVDF/PE membranes exhibit markedly different crystalline structure, as their XRD spectra display only one strong crystalline reflection at a scattering angle of ∼20.58 ± 0.05°, typical of the sum of the diffraction in the (110) and (200) planes of the β-phase[29,31,37] (Table 3). FT-IR corroborates the variation in the PVDF crystalline structure due to PE incorporation in the PVDF/PE membranes (Figure 8b), as the spectra display absorption bands at 445, 472, 490, and 842 cm^{-1}, including the ferroelectric all-trans conformation CF_2 bending band at 510 cm^{-1}, distinctive of the β-phase.[31,41] The change of PVDF polymorph indicates a perturbation of PVDF crystalline structure due to the presence of PE. This change from a nonpolar α-phase to a polar β-phase is not unreasonable due to the polar nature of the PE. Similar behavior has been observed for PVDF in presence of polar media such as salts or other type of electrolytes.[43,44] In addition, β-phase formation is well-known for PVDF blends with PMMA and other carbonyl-containing polymers and has been shown to result from a strong intermolecular interaction.[27] It is not known, however, if the type of crystalline phase of the original PVDF (prior to blending with PE) and that of the PVDF in the final membranes have any particular effect on proton conductivity.

The strong inverse relationship between the conductivity of PVDF/PE membranes and some of the crystalline characteristics of the inert PVDF phase, as seen in Figure 7, suggests an important effect of the latter on the thermodynamics and kinetics of nanophase separation responsible for the formation of ion-conducting channels. Particularly,

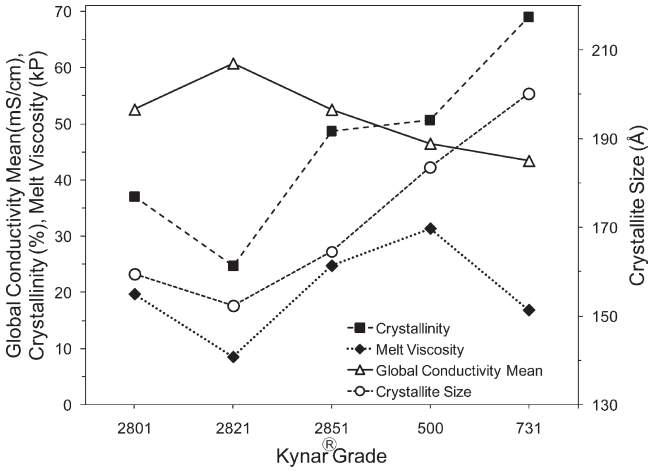

Figure 6. Comparison between global conductivity mean (unweighted mean) and PVDF crystallinity, crystallite size, and melt viscosity by PVDF type.

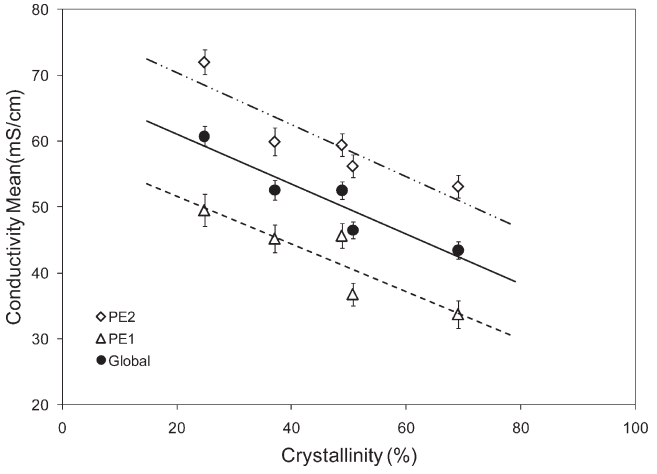

Figure 7. Comparison between global conductivity mean (unweighted mean) and PVDF crystallinity for PE1, PE2, and the global mean value of PE1 and PE2.

Table 3. WAXD of Pure PVDF Films and PVDF/PE[a] Films[b]

	hkl (020)		*hkl* (110)[c]		*hkl* (021)		*hkl* (200)[c]	
sample	2θ (deg)	*d* (Å)	2θ (deg)	*d* (Å)	2θ (deg)	*d* (Å)	2θ (deg)	*d* (Å)
Kynar 500	18.46	4.81	20.03	4.43	26.52	3.36	–	–
Kynar 731	18.47	4.80	19.99	4.44	26.54	3.36	–	–
Kynar 2801	18.34	4.84	19.85	4.47	26.68	3.34	–	–
Kynar 2821	18.32	4.84	19.79	4.49	26.53	3.36	–	–
Kynar 2851	18.40	4.82	19.97	4.45	26.80	3.33	–	–
Kynar 500/PE1	–	–	β→		–	–	20.61	4.31
Kynar 731/PE1	–	–	β→		–	–	20.55	4.32
Kynar 2801/PE1	–	–	β→		–	–	20.57	4.32
Kynar 2821/PE1	–	–	β→		–	–	20.51	4.33
Kynar 2851/PE1	–	–	β→		–	–	20.63	4.31

[a] Representative PVDF/PE films shown in this table correspond to membranes containing 50 wt % PE1. PVDF polymorph change from α to β phase was evident in all membranes containing either type of polyelectrolyte at all PVDF to PE ratios. [b] θ = Bragg angle and *d* = interplanar spacing. [c] Reflections from the sum of the diffractions in planes (110) and (200) for β-phase PVDF are shown in the column corresponding to plane (200); plane (100) reflections are denoted as "β→" for this phase.

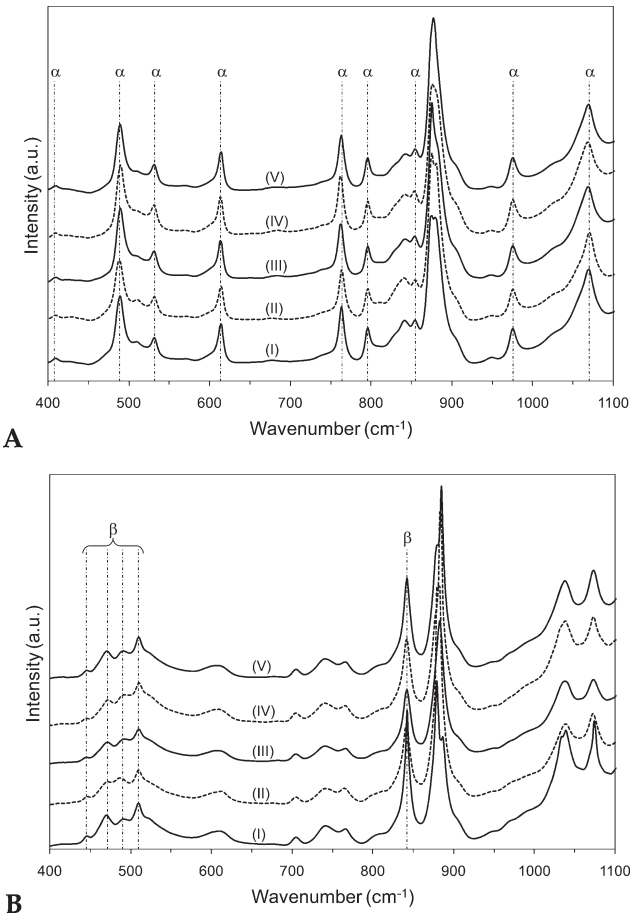

Figure 8. FT-IR spectra in the range of 400−1100 cm^{-1}. (A) NMP solvent-cast Kynar PVDF: (I) 500, (II) 731, (III) 2801, (IV) 2821, and (V) 2851. Vertical lines indicate typical α-phase absorption bands. (B) Kynar PVDF/PE1 membranes (only representative spectra of membranes containing 50 wt % neutralized form PE1 are shown. Membranes containing PE2 and different PE mass fractions exhibited identical behavior): (I) 500/PE1, (II) 731/PE1, (III) 2801/PE1, (IV) 2821/PE1, and (V) 2851/PE1. Vertical lines indicate typical β-phase absorption bands.

we hypothesize that the curing process (~20 min) is too short to allow for long-range rearrangement of the PVDF polymer chains. As a result, areas corresponding to locations where crystallites were initially situated before melting remain densely packed with PVDF chains throughout the curing process. These dense PVDF areas constitute an impediment for the segmental motion of PE chains that hampers their rearrangement and interconnection during cross-linking (Figure 9), resulting in less branched and interconnected proton conducting channels that are likely responsible for reduced conductivity. A similar structural effect has been observed previously in Nafion and Surlyn ionomers, where ionic species are excluded from crystalline domains.[45] What is more, decreased PE mobility and rearrangement are seemingly exacerbated by a synergistic effect between crystallinity and the high melt viscosity of the PVDF (Figure 6)—namely, Kynar 500, 31.42 kP; Kynar 731, 16.92 kP; Kynar 2801, 19.77 kP; Kynar 2821, 8.60 kP; and Kynar 2851, 24.80 kP—which might explain why Kynar 500 has a lower average conductivity than Kynar 2851, regardless of an almost identical crystallinity (50.69% vs 48.78%). Also, despite having a lower melt viscosity when compared to Kynar 500, it is important to remember that Kynar 731 is not completely molten throughout the curing process giving

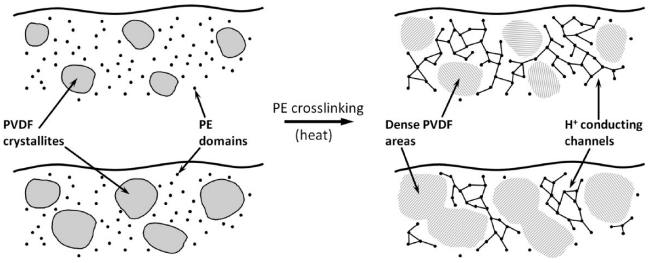

Figure 9. Schematic of the morphology transition of a solvent-based PVDF/PE blend containing individual PE domains and PVDF crystallites into a membrane of semi-interpenetrated PVDF structures and cross-linked proton conducting channels, after heat-induced cross-linking. The upper and bottom images correspond to low and high crystallinity PVDF, respectively, illustrating the effect of crystallinity and crystallite size in the formation of proton conducting channels.

rise to a possible competition between PVDF crystallization and PVDF−PE phase separation, as previously stated. The effect of reduced mobility of PE chains in high crystallinity PVDF matrices is further supported by the size of the PE clusters formed at high polyelectrolyte mass fractions (Figure 3); namely, clusters in the lower crystallinity PVDF:HFP copolymers reached a maximum size of ~450 nm for 60 wt % PE and ~410 nm for 55 wt % PE, whereas the maximum cluster size for a 60 wt % PE in any of the homopolymers was only on the order of ~355 nm.

Albeit longer curing/heating time periods may seem a reasonable approach to improve the conductivity of membranes manufactured with highly crystalline PVDF, it proved ineffective since the length of the curing process follows the completion of the PE cross-linking reaction (see Experimental Section, membrane preparation). Consequently, the network of cross-linked proton-conducting channels is already formed after 20 min, and further heating does not have a considerable effect on the PE network configuration. Additional annealing of finished membranes at the PVDF α-phase relaxation temperature (~90 °C) and above (130 and 170 °C) for 5 and 11 h proved to be equally unsuccessful. That is, no statistically significant increase in conductivity was observed in membranes annealed at 90 °C, whereas annealing at 130 and 170 °C was prominently detrimental for proton conductivity regardless of the duration (Supporting Information, inset Figure S2). The decrease in conductivity was accompanied by a manifest change in the PVDF crystalline phase evident from the FT-IR spectra of annealed membranes (Supporting Information, Figure S2). Specifically, the spectra of membranes annealed at 130 °C exhibit IR band broadening compared to the spectrum of a nonannealed reference membrane, while membranes annealed at 170 °C display a mix of α- and β-phase structures. In contrast, the FT-IR spectra of membranes annealed at the α-phase relaxation temperature virtually overlap with the spectrum of the nonannealed reference membrane (β-phase). The manifestation of IR broadening is perhaps explained by dipolar interactions[47] and may indicate the onset of the partial ferroelectric to paraelectric transition seen at 170 °C. Presumably, the associated decrease in conductivity can be attributed to PVDF segregation toward the membrane surface during annealing, resulting in a low surface energy polymer-rich layer depleted of ionic domains (similar to fluorine-rich layers found on the surface of Nafion[45]). This hypothesis coincides with a manifest strong wettability reduction (dry surface) noticed in membranes annealed at 130 and 170 °C. As temperature increased from 130 to 170 °C, the low-energy PVDF layer thickened, hindering conductivity even further and allowing the formation of

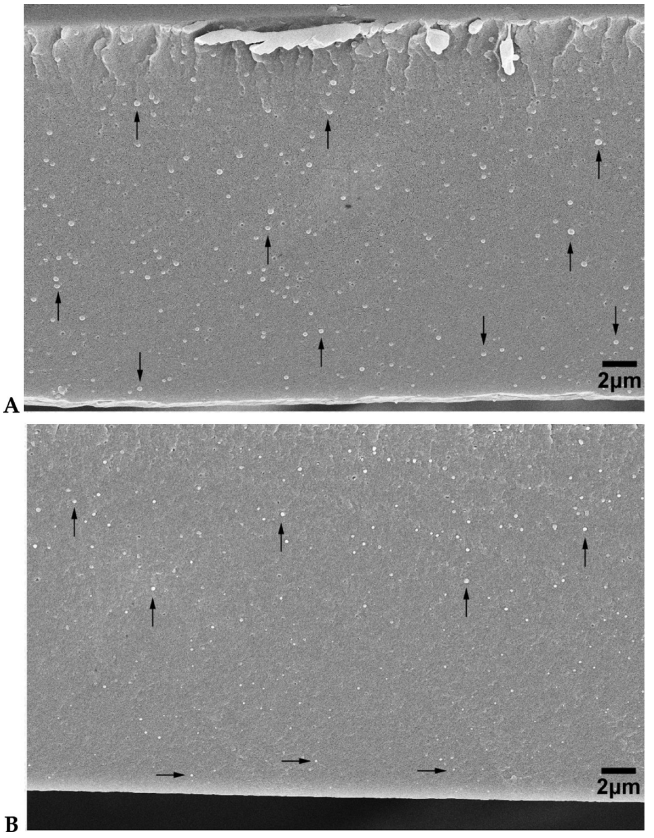

Figure 10. SEM images (EHT 10 kV) of the cross-sectional area of Kynar 731/PE1 (60 wt %) membranes: (A) nonannealed and (B) annealed at 170 °C. The nonannealed sample displays well-distributed PE clusters (vertical arrows) across the membrane thickness, whereas the annealed sample exhibits a noticeable PE cluster size and number distribution from big and numerous (vertical arrows) to small and scarce (horizontal arrows) toward the membrane surface.

nonpolar α-phase PVDF away from PE domains. What is more, SEM imaging of high PE concentration membranes annealed at elevated temperatures displays a perceptible reduction of PE clusters toward the membranes surface (Figure 10), which might indicate the speculated formation and thickening of a PVDF-rich layer. A gradual color progression (from clear to brownish) of the membranes was noticed as well with increasing annealing temperature, suggesting the formation of conjugated C=C bonds arising from PVDF dehydrofluorination in the presence of PE.

Supplementary crystallinity characterization of the different PVDF grades, particularly, the crystallite thickness distribution and transition layers between the amorphous and crystalline domains, can be carried out via small-angle X-ray scattering (SAXS) long-period measurements (not performed in this study) to further elaborate on the relationship between crystalline properties of PVDF and proton conductivity of PVDF/PE membranes.

In general, lower PVDF crystallinity translates into higher proton conductivity. In fact, contrary to what would be the conventional approach to enhance proton conductivity by only increasing the content of PE, the results suggest that the use of other PVDF grades with lower crystallinity (e.g., copolymers with higher content of HFP) for the manufacturing of the membranes could be a plausible method to boost conductivity (especially as there is no statistically significant conductivity rise above 55 wt % PE). In addition, prolonged heat pretreatment (prior to PVDF−PE blending) of highly crystalline PVDF types above their melting temperature,

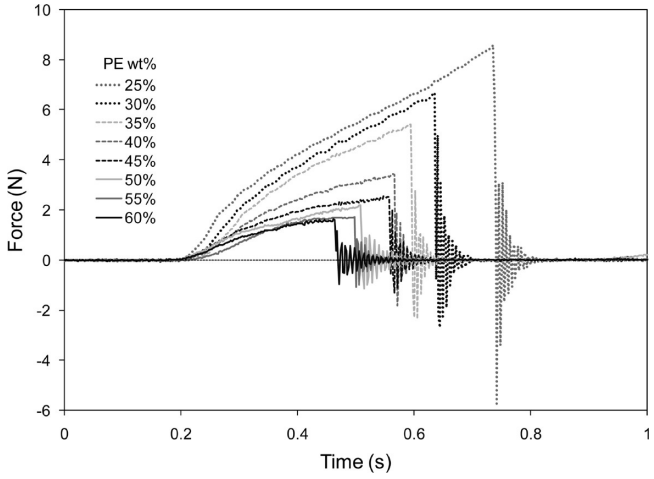

Figure 11. Representative HTMECH force vs time profiles of PVDF/PE membranes. The arrow indicates the direction in which the mass fraction of PE decreases. Profiles correspond to Kynar 2851/PE2 membranes.

followed by ultrafast quenching to preclude crystallite growth, could serve to circumvent the unfavorable effect of high crystallinity on conductivity, allowing the use of these PVDF types in the manufacturing of PVDF/PE membranes with adequate proton conductivity. However, besides proton conductivity, the use of a particular PVDF type is also constrained by the required mechanical and fuel barrier properties of the membrane.

Mechanical Properties. Representative force vs time profiles from HTMECH characterization of PVDF/PE membranes are shown in Figure 11 (~1750 total profiles were analyzed for this study). Contrary to uniaxial deformation typical of conventional mechanical characterization, membranes undergo axisymmetric biaxial deformation in HTMECH tests. A possible advantage of this type of deformation may be the reduction of structural anisotropy effects, related to potential uneven distributions of PVDF-rich domains and cross-linked PE structures, on the measured membrane properties. However, care must be taken if the results are to be compared to uniaxial tensile tests. For instance, the biaxial "engineering" elastic modulus obtained from HTMECH characterization is predicted to be approximately twice the Young's modulus measured under uniaxial tension.[47] In addition, other geometry-dependent factors, such as nonaffine membrane deformation arising from the very dissimilar mechanical characteristics of the blend components (i.e., PVDF and acrylic PE) and nonlinear stress response, might increase the difference between biaxial and uniaxial characterization approaches. To simplify the analysis model, the membrane was assumed to adopt a linear profile under deformation. Additional considerations about the HTMECH system and testing methodology can be found elsewhere.[21,48]

The mechanical properties of PVDF/PE1 membranes are shown in Figure 12 (data for PE2-containing membranes follow similar trends, Supporting Information, Figure S3). A GLM statistical analysis tests revealed statistically significant effects of PE content ($F_{(7,1657)} = 940.4$, $p < 0.001$), PE type ($F_{(1,1657)} = 207.6$, $p < 0.001$), and PVDF grade ($F_{(4,1657)} = 349.5$, $p < 0.001$) on membrane elastic modulus; significant effects of PE content ($F_{(7,1657)} = 799.9$, $p < 0.001$), PE type ($F_{(1,1657)} = 106.9$, $p < 0.001$), and PVDF grade ($F_{(4,1657)} = 291.6$, $p < 0.001$) on membrane ultimate tensile strength; as well as significant effects of PE content ($F_{(7,1657)} = 396.9$, $p < 0.001$), PE type ($F_{(1,1657)} = 53.9$,

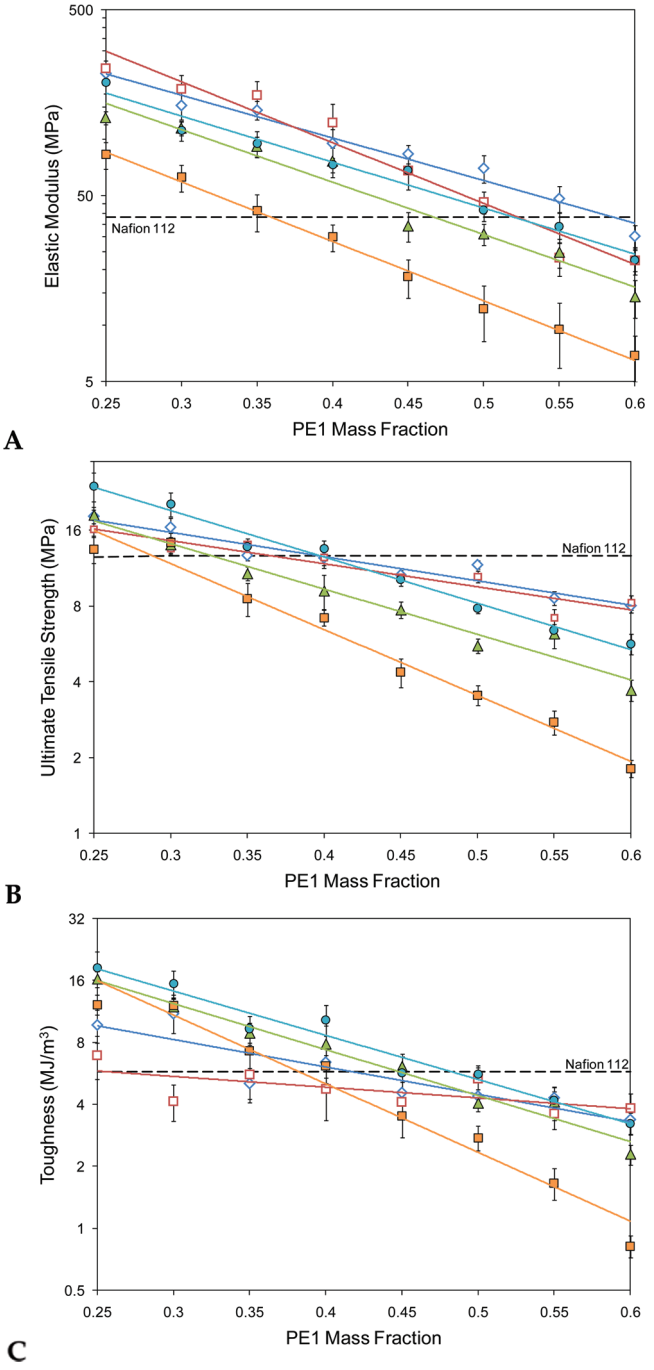

Figure 12. Parametric plots of mechanical properties for Kynar PVDF/PE1 membranes at various Kynar grades (500, ◇; 731, □; 2801, ▲; 2821, ■; and 2851, ●) and polyelectrolyte mass fractions. Mechanical properties include biaxial elastic modulus (A), ultimate tensile strength (B), and toughness (C). Horizontal dotted lines in each plot correspond to the reference value of Nafion 112. All membranes were tested in a hydrated state. Polyelectrolyte content is expressed as the mass fraction of neutralized form polyelectrolyte in the final membrane. Values are averages ±95% confidence intervals. All plots are presented in a logarithmic scale.

$p < 0.001$), and PVDF grade ($F_{(4,1657)} = 91.8$, $p < 0.001$) on membrane toughness. Significant interaction effects of each of the factors exist as well for all the mechanical properties ($p < 0.001$) and were corroborated by subsequent simple effects analysis (data not shown).

Although a significant factor, the size effect of the PE type on the mechanical properties is weak ($0.03 \leq \eta_{p^2} \leq 0.11$), which was evident in the simple effects analysis where at several fixed levels of PVDF type and PE content the difference in mechanical behavior of PE1 and PE2 membranes was statistically negligible. This was anticipated as the mechanical strength of both PE types is extremely low when compared to that of PVDF; consequently, the effect of PE on mechanical properties depends on the amount of PVDF it "displaces", thus weakening the membrane.

Homopolymer-based membranes exhibited the highest elastic moduli over the range of PE mass fractions in comparison with copolymer-based ones. This is attributed to the added flexibility in the copolymer chains due to HFP comonomers. Similarly, the ultimate tensile strength of the PVDF/PE membranes was generally higher for those containing PVDF homopolymers. Only at very small PE mass fractions did some copolymers, particularly Kynar 2851, exhibit a higher tensile strength. This coincides with the appearance of a slope increment beyond the initial plastic flow at the end of force vs time profiles, consistent with strain-induced crystallization of copolymer-based membranes at low PE content. Opposite to general trends in elastic moduli, toughness was higher in the copolymer-based membranes between low and medium PE mass fractions, owing to a more flexible structure of the copolymer PVDF matrix that allows for better absorption of the impact energy (higher resistance to failure). Interestingly, toughness in the homopolymer-based membranes seems to diminish at a slower pace than for the copolymer-based ones (smaller slope), being higher for the former above medium PE mass fractions. This might be related to added ductility to the PVDF matrix by the PE domains that allow for better impact energy dissipation and improved membrane failure threshold. In fact, addition of PE to homopolymer-based membranes resulted in improved strain at break (not shown), whereas the presence of PE was always detrimental for strain at break of copolymer-based membranes, suggesting a different interaction mechanism between the PVDF and PE phases in homo- and copolymer-based membranes. Presumably, this difference may be rooted on the previously proposed model of variable distribution of PE and PVDF domains that depends on the inert matrix original crystallinity and crystallite size as well as melt viscosity (Figure 9).

A remarkably good exponential-decay fit, analogous to the Maxwell model for polymer stress and strain behavior as a function of time, was found for all the mechanical properties as a function of the PE mass fraction (trendlines in Figure 12). Although similar exponential decaying relationships exist for the yield stress of polymer suspensions as a function of the suspension concentration,[49] we are not aware of any blend model, or experimental studies for that matter, that elucidate the nature of this particular type of mechanical property/composition association. Interestingly, the goodness of fit of the exponential profiles of the homopolymers was on average lower than that of the copolymers, alluding to the model of dissimilar interaction mechanisms between PE and PVDF homo- and copolymers. In contrast, no defined relationships were found for membrane conductivity as a function of PE content (the best approximations corresponded to quadratic models; however, correlation coefficients were particularly low: < 0.7).

Figure 13 presents contour maps of conductivity and ultimate tensile strength for PE1. The contour maps represent response surfaces that can be used in membrane optimization and design. In general, opposite to the conductivity behavior, copolymer-based membranes exhibited the lowest mechanical properties. In fact, membranes containing Kynar 2801, which attained the highest average conductivity, had the lowest average elastic modulus, ultimate tensile

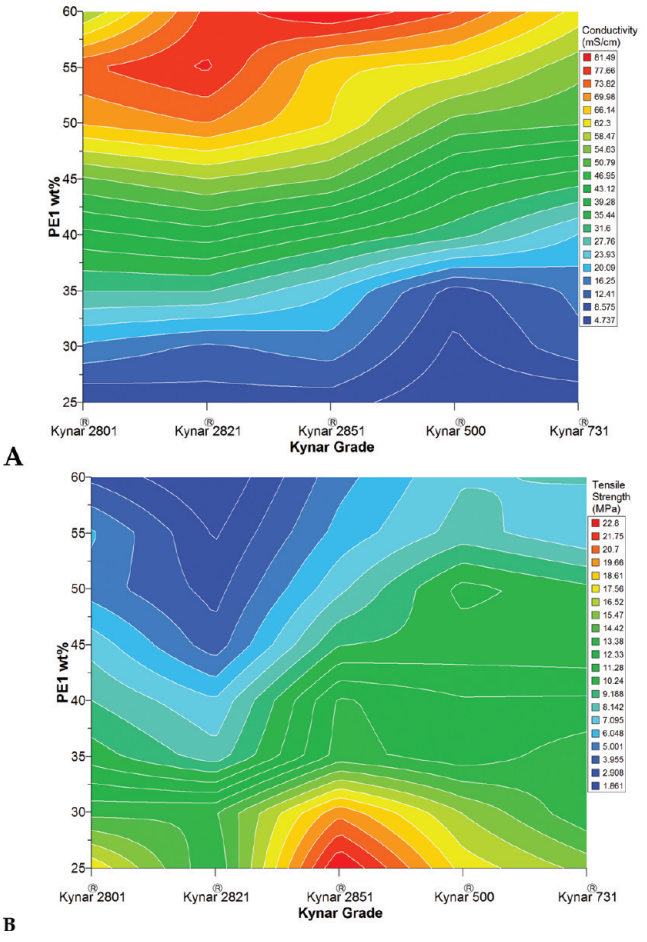

Figure 13. Contour maps for (A) conductivity and (B) ultimate tensile strength for PE1−Kynar membranes, illustrating the nonlinear response surface and opposing trends for these two properties.

strength, and toughness. It is important to notice, however, that in the dry state copolymer-based membranes were less brittle and more easily handled than homopolymers. When compared to the average Nafion 112 mechanical properties (horizontal reference line in Figure 12 and Figure S3 of the Supporting Information), the PVDF/PE membranes perform satisfactorily, having a similar average range of mechanical properties at medium PE mass fractions. On the contrary, at low PE contents the mechanical properties of PVDF/PE membranes can reach values as high as 5 times (elastic modulus), 2 times (ultimate tensile strength), or 3 times (toughness) those in Nafion 112 due to the high PVDF to PE ratio. At a glance membranes containing Kynar 2801 or 2851 and PE2 in the range of 40−50 wt % provide the best trade-off of conductivity and mechanical properties, whereas Kynar 2821 and 500 provide the best individual conductivity and mechanical properties, respectively.

Conclusions

Novel membranes of semi-interpenetrated networks of Kynar PVDF and covalently cross-linked sulfonated acrylic polyelectrolytes were prepared from five different Kynar PVDF grades and two polyelectrolytes blended at numerous Kynar to PE ratios. The proton conductivity and mechanical properties of the membranes were assayed by means of custom-designed electrochemical impedance spectroscopy and biaxial axisymmetric deformation high-throughput screening tools (HTC and HTMECH), respectively.

As anticipated, membrane conductivity was higher in membranes containing PE with lower equivalent weight and increased as the amount of PE increased. Statistical analysis of the conductivity data revealed a maximum effective amount of polyelectrolyte of approximately 55−60 wt %, above which there was no statistically significant change in conductivity. This conductivity plateau was linked to the coalescence of ion conducting domains at high PE mass fractions in the membrane. In addition, even though a considerable decoupling of proton conductivity from the properties of the inert phase was initially expected, a significant effect of Kynar PVDF grade indicated that conductivity was strongly favored in membranes containing PVDF:HFP copolymers in comparison to those containing PVDF homopolymers. Further analysis revealed a direct correlation between proton conductivity and several physical properties of the PVDF phase such as crystallinity, crystallite size, and melt viscosity. Specifically, conductivity was found to decrease with increased crystallinity, crystallite size, and melt viscosity of the PVDF phase. The maximum overall conductivity was attained by membranes containing Kynar 2821 PVDF:HFP copolymer (X_C = 24.8%, D = 152.4 Å, η_M = 8.6 kP), while the lowest by those based on Kynar 731 PVDF homopolymer (X_C = 69.1%, D = 200.2 Å, η_M = 16.9 kP). A model based on the impediment of the PE segmental motion during the cross-linking process by a synergistic effect of high viscosity and dense PVDF areas formed by molten crystallites is proposed to explain this behavior. Annealing of PVDF/PE membranes at temperatures above the PVDF α-phase relaxation temperature resulted in the apparent formation of a PVDF-rich surface layer exhibiting a partial ferroelectric to paraelectric phase transition, accompanied by a substantial reduction of proton conductivity.

Mechanical properties were mainly dictated by the PVDF grade. Elastic modulus and ultimate tensile strength were generally higher in membranes containing stiffer PVDF homopolymers than in those that incorporate more flexible PVDF:HFP copolymers (only in a few cases at low PE content copolymer-based membranes exhibited higher tensile strength as a result of strain-induced crystallization). Toughness was higher in copolymer-based membranes in the range of low to medium PE content (25−45 wt %) due to the ability of the more flexible PVDF:HFP system to absorb the impact energy of the test.

In general, PVDF/PE membranes compare favorably against Nafion 112, reaching conductivities as high as 130 mS/cm (at 25 °C in water) and mechanical properties that can be several times higher than those of Nafion 112. However, the selection of a particular PVDF/PE membrane, and hence the trade-off between conductivity and mechanical characteristics, will be dictated by the requirements of its final application.

Acknowledgment. We gratefully acknowledge the help from Mr. Jung-Hyun Lee for SEM imaging and funding from the US Department of Energy (DE-SC02-03CH11137).

Supporting Information Available: DSC heating profiles of Kynar PVDF powders, FT-IR spectra of PVDF/PE membranes annealed at 90 °C, 130 and 170 °C, and parametric plots of mechanical properties for Kynar PVDF/PE2 membranes at various Kynar grades and polyelectrolyte mass fractions. This material is available free of charge via the Internet at http://pubs.acs.org.

References and Notes

(1) Cropper, M. A. J.; Geiger, S.; Jollie, D. M. *J. Power Sources* **2004**, *131*, 57–61.
(2) Sopian, K.; Daud, W. R. W. *Renewable Energy* **2006**, *31*, 719–727.
(3) Kerres, J. A. *J. Membr. Sci.* **2001**, *185*, 3–27.
(4) Johnston, B.; Mayo, M. C.; Khare, A. *Technovation* **2005**, *25*, 569–585.

(5) Hart, D. *J. Power Sources* **2000**, *86*, 23–27.
(6) Whittingham, M. S.; Savinell, R. F.; Zawodzinski, T. *Chem. Rev.* **2004**, *104* (10), 4243–4244.
(7) Kerres, J. A. *Fuel Cells* **2005**, *5* (2), 230–247.
(8) Meier-Haack, J.; Taeger, A.; Vogel, C.; Schlenstedt, K.; Lenk, W.; Lehmann, D. *Sep. Purif. Technol.* **2005**, *41*, 207–220.
(9) Kreuer, K.-D.; Paddison, S. J.; Spohr, E.; Schuster, M. *Chem. Rev.* **2004**, *104* (10), 4637–4678.
(10) Hickner, M. A.; Ghassemi, H.; Kim, Y. S.; Einsla, B. R.; McGrath, J. E. *Chem. Rev.* **2004**, *104*, 4587–4612.
(11) Hickner, M. A.; Pivovar, B. S. *Fuel Cells* **2005**, *5* (2), 213–229.
(12) Cho, C. G.; Kim, S. H.; Park, Y. C.; Kim, H.; Park, J.-W. *J. Membr. Sci.* **2008**, *308*, 96–106.
(13) Swier, S.; Ramani, V.; Fenton, J. M.; Kunz, H. R.; Shaw, M. T.; Weiss, R. A. *J. Membr. Sci.* **2005**, *256* (1−2), 122–133.
(14) Arnett, N. Y.; Harrison, W. L.; Badami, A. S.; Roy, A.; Lane, O.; Cromer, F.; Dong, L.; McGrath, J. E. *J. Power Sources* **2007**, *172*, 20–29.
(15) Mokrini, A.; Huneault, M. A.; Gerard, P. *J. Membr. Sci.* **2006**, *283*, 74–83.
(16) Fu, R.-Q.; Julius, D.; Hong, L.; Lee, J.-Y. *J. Membr. Sci.* **2008**, *322*, 331–338.
(17) Moszczyński, P.; Kalita, M.; Parzuchowski, P.; Siekierski, M.; Wieczorek, W. *J. Power Sources* **2007**, *173*, 648–656.
(18) Quartarone, E.; Carollo, A.; Tomasi, C.; Belotti, F.; Grandi, S.; Mustarelli, P.; Magistris, A. *J. Power Sources* **2007**, *168*, 126–134.
(19) Sormana, J.-L.; Chattopadhyay, S.; Meredith, J. C. *Rev. Sci. Instrum.* **2005**, *76*, 062214.
(20) Zapata, P.; Basak, P.; Meredith, J. C. *Electrochim. Acta* **2009**, *54* (15), 3899–3909.
(21) Whitacre, J. F.; Valdez, T. I.; Narayanan, S. R. *Electrochim. Acta* **2008**, *53*, 3680–3689.
(22) Humphrey, J. S.; Gaboury, S. R. U.S. Patent #5,922,493.
(23) Choi, N.-S.; Lee, Y. M.; Seol, W.; Lee, J. A.; Park, J.-K. *Solid State Ionics* **2004**, *172*, 19–24.
(24) Gozdz, A. S.; Schmutz, C. N.; Tarascon, J.-M.; Warren, P. C. U.S. Patent #5,418,091.
(25) Meredith, J. C.; Karim, A.; Amis, E. J. *MRS Bull.* **2002**, *27* (4), 330–335.
(26) Meredith, J. C.; Smith, A. P.; Karim, A.; Amis, E. J. *Macromolecules* **2000**, *33*, 9747–9756.
(27) Kim, K. J.; Cho, Y. J.; Kim, Y. H. *Vib. Spectrosc.* **1995**, *9*, 147–159.
(28) Jayasuriya, A. C.; Schirokauer, A.; Scheinbeim, J. I. *J. Polym. Sci., Part B: Polym. Phys.* **2001**, *39*, 2793–2799.
(29) Gregorio, R. J.; Ueno, E. M. *J. Mater. Sci.* **1999**, *34*, 4489–4500.
(30) Wang, Y.; Cakmak, M.; White, J. L. *J. Appl. Polym. Sci.* **1985**, *30*, 2615–2632.
(31) Gregorio, R. J. *J. Appl. Polym. Sci.* **2006**, *100*, 3272–3279.
(32) Mhalgi, M. V.; Khakhar, D. V.; Misra, A. *Polym. Eng. Sci.* **2007**, *47* (12), 1992–2004.
(33) Newman, B. A.; Scheinbeim, J. I. *Macromolecules* **1983**, *16*, 60–68.
(34) Moggi, G.; Bonardelli, P.; Bart, J. C. J. *Polym. Bull.* **1982**, *7*, 115–122.
(35) Cui, Z.-Y.; Xu, Y.-Y.; Zhu, L.-P.; Deng, H.-Y.; Wang, J.-Y.; Zhu, B.-K. *J. Macromol. Sci., Part B: Phys.* **2009**, *48*, 41–54.
(36) Tazaki, M.; Wada, R.; Okabe, M.; Homma, T. *J. Appl. Polym. Sci.* **1997**, *65*, 1517–1524.
(37) Satapathy, S.; Gupta, P. K.; Pawar, S.; Varma, K. B. R. arXiv:0808.0419v1, **2008**.
(38) Birkholz, M. *Thin Film Analysis by X-Ray Scattering*; Wiley-VCH Verlag GmbH & Co. KGaA: Weinheim, 2006; p 378.
(39) Kong, Y.; Hay, J. N. *Eur. Polym. J.* **2003**, *39*, 1721–1727.
(40) Cao, J.-H.; Zhu, B.-K.; Xu, Y.-Y. *J. Membr. Sci.* **2006**, *281*, 446–453.
(41) Bachmann, M. A.; Gordon, W. L.; Koenig, J. L.; Lando, J. B. *J. Appl. Phys.* **1979**, *50*, 6106–6112.
(42) Lovinger, A. J. *Science* **1983**, *220* (4602), 1115–1121.
(43) Abbrent, S.; Plestil, J.; Hlavata, D.; Lindgren, J.; Tegenfeldt, J.; Wendsjö, Å. *Polymer* **2001**, *42*, 1407–1416.
(44) Jiang, Z.; Carroll, B.; Abraham, K. M. *Electrochim. Acta* **1997**, *42* (17), 2667–2677.
(45) McLean, R. S.; Doyle, M.; Sauer, B. B. *Macromolecules* **2000**, *33*, 6541–6550.
(46) Painter, P. C.; Pehlert, G. J.; Hu, Y.; Coleman, M. M. *Macromolecules* **1999**, *32* (6), 2055–2057.
(47) Sormana, J.-L.; Meredith, J. C. *Macromol. Rapid Commun.* **2003**, *24* (1), 118–122.
(48) Sormana, J.-L.; Meredith, J. C. *Macromolecules* **2004**, *37* (6), 2186–2195.
(49) Utracki, L. A. *Polymer Blends Handbook*; Springer-Verlag: New York, 2003; p 1442.